Contact delamination detection of anisotropic composite plates using non-elliptical probability imaging of nonlinear ultrasonic guided waves

Yuan Liu, Xiaobin Hong and Bin Zhang

Abstract

Contact delamination damage easily occurs inside the composite. The extension and accumulation of the damage occupy most of the time from damage appearance to failure. However, the anisotropy of materials and the small size of early damage make accurate detection difficult. In this paper, a non-elliptical probability imaging (NEPI) method based on nonlinear ultrasonic guided waves is proposed for the delamination damage detection in anisotropic composites. Firstly, the anisotropic characteristics of the composite are analyzed theoretically, and the velocity in all directions is obtained by numerical simulation. Secondly, the arrival time is obtained by the intersection of the upper and lower envelope fitting lines, and nonlinear coefficient is calculated based on the smooth pseudo Wigner–Ville distribution (SPWVD). Then, the time coefficient (C_T) and nonlinear damage index (NDI) are defined and applied in the NEPI. By comparison with a reference point, the problem that the damage location of anisotropic composite cannot be solved analytically is avoided skillfully. Finally, the NEPI method is used to present the damage. The experiment results show that the NEPI method can accurately display the damage location. The sensitivity and reliability of NDI based on SPWVD are further verified by comparison with damage index of scattered signal and time–frequency analysis methods such as fast Fourier transform, short-time Fourier transform, and S-transform. The proposed NEPI method based on nonlinear ultrasonic guided waves can detect the delamination damage with good location accuracy and high damage sensitivity.

Keywords

Anisotropic composite, Nonlinear ultrasonic guided waves, Non-elliptical probability imaging, Contact delamination detection, smooth pseudo Wigner–Ville distribution

Introduction

Composite materials have been widely used in engineering structures for its excellent comprehensive properties. As an advanced composite material, the carbon fiber composite has excellent weight reduction function on the basis of ensuring material performance. These engineering structures are usually in service for several years to decades. Due to the different material properties, delamination damage easily occurs inside the materials during the long service period. With the damage propagation, the integrity of the material is seriously destroyed, and the performance decreases sharply. The extension and accumulation of damage occupy most of the time from damage appearance to failure. Therefore, it is of great significance to develop an effective early structural damage detection method for composite materials.

During nondestructive evaluation[1–3] and structural health monitoring,[4–7] ultrasonic guided-wave detection technology has been widely used for its high detection sensitivity and efficiency. In most of the literatures, the changes of linear time-domain characteristics in amplitude and phase, such as wave reflections,[8,9] energy transfer,[10,11] and time of flight,[12,13] are used to monitor and evaluate the damage. However, limited by the wavelength, the linear

School of Mechanical & Automotive Engineering, South China University of Technology, Guangzhou, China

Corresponding author:
Xiaobin Hong, School of Mechanical & Automotive Engineering, South China University of Technology, 381 Wushan Road, Tianhe District, Guangzhou, China.
Email: scut_hongxiaobin@126.com

time-domain characteristics are not sensitive to the small defects or the damage with weak reflection echo such as fatigue cracks and delamination. This makes the detection of those damages very difficult. The appearance of nonlinear ultrasonic guided wave brings great convenience for early damage monitoring. The nonlinear ultrasonic guided wave can achieve the detection of early micro damage effectively through the nonlinear effect produced by the interaction between the finite amplitude acoustic wave and the microdamage.[14,15] Tian et al.[16] employed nonlinear ultrasonic guided wave method to detect the fatigue cracks, and an aluminum–lead composite material was designed to improve the detection effect by eliminating inherent nonlinear components. Zhao et al.[17] investigated the relationship between the higher harmonic and delamination length of composite double cantilever beams, and found that the higher harmonics appeared with the introduction of the nonlinear contact. Sharif-Khodaei et al.[18,19] presented a multi-level decision fusion strategy, which can realize the existence, location, and imaging detection of barely visible impact damage in composite materials according to the demand. Yang et al.[20] analyzed the influence of the wave mode on the harmonic, and found that the magnitude and directivity of the harmonic are related to the ratio of crack length to incident wavelength and the ratio of S_0 to A_0 incident Lamb wave amplitude. Mostavi et al.[21] established an immersion nonlinear ultrasonic system to measure the plastic deformation of aluminum, which could significantly improve the detection sensitivity for micro damage. Shen et al.[22,23] designed the fusion damage index from three aspects of time: history, amplitude, and nonlinear resonance. The nonlinearity of the fatigue crack of a rivet hole was studied under the condition of a rough contact surface. Hong et al.[24–26] applied the nonlinear ultrasonic guided wave technology to monitor civil equipment such as glass curtain wall and anti-corrosion pipes, and the results showed that the nonlinear damage index can represent the change of damage. However, compared with linear features, nonlinear features are very weak. In addition, the nonlinear features are obtained in the frequency domain, and the time information of the signal is lost. This makes it difficult to locate and image the damage even if the damage can be detected by the nonlinear ultrasonic guided wave detection technology.

A probabilistic imaging method can achieve a higher damage imaging effect through a sparse sensor network with fewer sensors, which sets off a boom of imaging detection, and provides a good opportunity for nonlinear damage imaging detection. Lee et al.[27] developed a probability damage detection reconstruction algorithm to address the guided wave imaging; a shape factor related to path distance is used to improve the probability accuracy.

Hua et al.[28] enhanced the probability reconstruction imaging effect by extracting the local lamb wave signal as signal characteristic, which could exclude the background noise of invalid paths. Wang et al.[29] calculated the damage probability value based on the correlation analysis, and the virtual paths are added to improve the imaging quality. Furthermore, the effect of temperature on the damage characteristics was studied, and Shannon entropy was employed to improve the robustness of the imaging algorithm.[30] Liu et al.[31] applied the Duffing chaotic oscillator in the probability imaging detection of composite materials, and the normalized Lyapunov exponent was used to calculate the damage probability. However, the probability value of this probability imaging method decreases linearly with the increase of path distance. The damage probability problem is always the largest on the path, which is not accurate. Some scholars have improved the probability imaging method and proposed the elliptical-based probability imaging method, which further improves the accuracy of damage location and imaging. Liu et al.[32] showed the damage location capability of the elliptical probability imaging method, and the probability determined by one path is distributed in an elliptical ring. Hong et al.[33,34] combined nonlinear ultrasonic guided waves and elliptical probability imaging technology, and the accurate location of small size fatigue crack is realized. Zeng et al.[35] increased the number of sensing paths by adding virtual sensors, and combined with probabilistic imaging technology, to realize damage detection and location with a pair of excitation-receiving transducers. However, the composite material is anisotropic and non-uniform; its wave velocity varies with directions. The sum of the distance from the damage to the excitation and the receiving transducer is not a fixed value, and the elliptical damage path cannot be obtained by an analytic method. Even if the velocities are known, it is still impossible for the ellipse-based probability imaging (EPI) method to realize the damage location and imaging of anisotropic composite materials.

At present, a solution strategy is to transform the damage location problem of anisotropic composite structures into an optimization problem. Moll et al.[36] proved mathematically that the ellipse probability imaging technique cannot be directly solved analytically in the damage location of anisotropic composite materials. Then, the spectral element method combined with 2D probability density function and expectation maximization algorithm was applied to address this problem. Kundu et al.[37] transformed the impact location problem of anisotropic composite plate into an optimization problem of minimum error function to avoid the direct solution of impact location. However, the methods mentioned above need sufficient theoretical basis and a lot of complex calculation. The author also proposed a probability imaging method that combines the velocity in all directions

of carbon composite material, and realized the accurate imaging characterization of crack damage.[38] However, there is still no good detection effect for the early structural damage of anisotropic composites.

In this paper, a non-elliptical probability imaging (NEPI) technology combined with wave velocity of all directions based on nonlinear ultrasonic guided waves was studied to detect the early structural damage of anisotropic composite materials accurately. The velocity in different directions of anisotropic structure is considered, which provides more accurate time information. By setting the reference point and comparing the reference point with the damage, the analytic solution process of the damage location is cleverly avoided. Furthermore, nonlinear ultrasound is introduced to improve the detection ability. The main contents of this paper are as follows: First, the dispersive nature of anisotropic composite and the theoretical basis of nonlinear ultrasonic guided waves are introduced. Second, the implementation process of NEPI combined with the velocity of all directions is presented. Then, the simulation model of the contact delamination anisotropic composite plate is established. Finally, a nonlinear ultrasonic guided wave detection platform for anisotropic composite plates is used to verify the early structural damage detection effect of the method.

Theory and methodology

Dispersion property of anisotropic composite plates

The composite plates are composed of fiber layers with different angles. Therefore, composite plates are anisotropic materials, and the stiffness matrix is different when the acoustic wave travels in different directions. The stiffness matrix of anisotropic composite plates in any direction can be expressed as follows

$$C = \begin{bmatrix} C_{11} & C_{12} & C_{13} & 0 & 0 & C_{16} \\ C_{12} & C_{22} & C_{23} & 0 & 0 & C_{26} \\ C_{13} & C_{23} & C_{33} & 0 & 0 & C_{36} \\ 0 & 0 & 0 & C_{44} & C_{45} & 0 \\ 0 & 0 & 0 & C_{45} & C_{55} & 0 \\ C_{16} & C_{26} & C_{36} & 0 & 0 & C_{66} \end{bmatrix} \quad (1)$$

Figure 1 shows the coordinate system and layering structure of a 15-layer anisotropic composite plate. The stacking sequence of CFRP plate is 0° and 90° alternately, which is expressed as $[0/90/_{\text{alternative}}.../0]_{15}$. The subscript 15 indicates the total number of anisotropic composite plate layers. β indicates the angle between the fiber direction and the propagation direction. When the acoustic wave propagates along the x or y axis, that is consistent with the fiber direction, C_{16}, C_{26}, C_{36}, and C_{45} in equation (1) are equal to
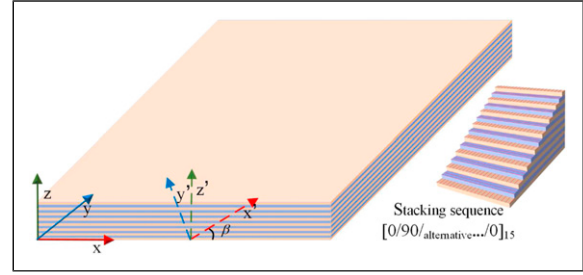

Figure 1. Coordinate system and layering structure of a 15-layer anisotropic composite plate.

zero. When the acoustic wave propagates along directions x', the stiffness matrix is related to the angle β between x and x'. The stiffness matrix of the wave propagates along the x' direction and along the x direction, can be converted by $C_{x'} = T(\beta)C_x T^{\mathrm{T}}(\beta)$. $T(\beta)$ is the transformation matrix related to the angle β, which is common in composite books.[39] The stiffness matrix of acoustic wave propagates in different directions and varies with the angle β, which is also the essential reason for the different velocities of acoustic waves in different directions. However, for ellipse-based probabilistic imaging technology, the velocity of acoustic waves is critical to imaging accuracy of anisotropic composite plates. Inaccurate velocity information will lead to some errors in damage location and imaging.

The dispersion curve of anisotropic composite plates can be calculated according to the material parameters. However, the calculation process is very complex, and the velocities in all directions need to be calculated separately. Moreover, there is always a deviation between the theoretical calculation results and the reality. On the other hand, the inconsistency of PZT, the difference of propagation distance, and attenuation rate will inevitably lead to errors, while those can be avoided in the simulation. Therefore, a velocity simulation with the same propagation distance from the receiving PZT to the excitation PZT was carried out to obtain the velocity in all directions. Carbon fiber–reinforced plastics (CFRP) with size 600 mm × 600 mm × 3 mm are considered in this paper. The total number of layers is 15, and the thickness of each layer is 0.2 mm. The parameters of CFRP are displayed in Table 1. According to the constitutive relationship of anisotropic composite, the stiffness matrix of the CFRP plate can be obtained. The software GUIGUW[40] can calculate the dispersion curve of anisotropic composite structure using the semi-analytical finite element (SAFE) method. GUIGUW is still being developed, and the current version can be used for free, which is suitable for this problem. A 15-layer composite plate structure is set in GUIGUW, the material is set to be anisotropic, and the stiffness matrix of CFRP plate is input. The "layer rotation" of each layer is set to 0° and 90° alternately, and the thickness is 0.2 mm. Figure 2 shows the

Table 1. The parameters of CFRP.

E_1 (GPa)	E_2 (GPa)	G_{12} (GPa)	G_{23} (GPa)	N_u	ρ (kg.m^{-3})	Stacking sequence
144.7	9.65	9.65	3.4	0.3	1500	$[0/90_{alternative}.../0]_{15}$
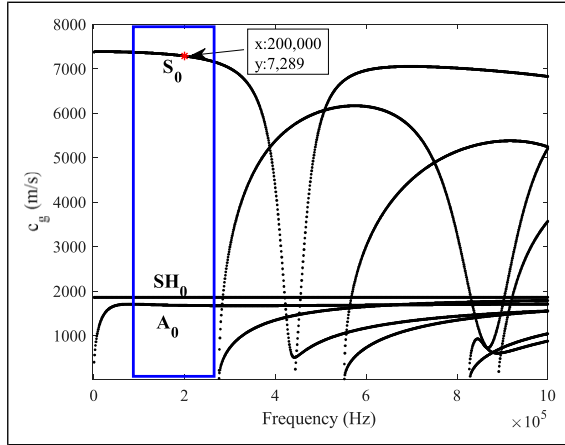
Figure 2. The group velocity dispersion curve of CFRP along the 0° direction.

group velocity dispersion curve of CFRP along the 0° direction. The excitation frequency of the guided wave in simulation and subsequent experiments is determined according to the group velocity dispersion curve of CFRP. It can be seen that when the frequency is lower than 300 kHz, there are fewer guided-wave modes, and the velocity is relatively stable. Therefore, the excitation frequency of the guided-wave signal is determined as 200 kHz. Among those modes, the velocity of S_0 mode is the fastest, which means that the interference of S_0 mode is the least in a relatively short time from receiving the signal.

The model of CFRP is established in ABAQUS (Abaqus Inc., CA, USA), which is shown in Figure 3(a). Signal excitation and receiving transducers are performed by lead zirconate titanate (PZT), which are also established in the model. The diameter of PZTs is 10 mm, and the thickness is 1 mm. All PZTs modules are constrained on the surface of the composite plate, and their distribution position is shown in Figure 3(a). The red one is the excitation PZT, right at the center of the composite plate. The excitation signal is a 5-peak sine wave with a frequency of 200 kHz and modulated by the Hanning window to make the signal energy more concentrated. Because the stacking sequence of the CFRP plate is $[0/90_{alternative}.../0]_{15}$, the receiving PZT is placed in the first quadrant according to its symmetry. The green ones are the receiving PZTs, evenly distributed on a circle 200 mm away from the excitation PZT. The position of the vertices of the CFRP is fully fixed. The purpose of the excitation PZT is to generate acoustic vibration signals, and the essence of applying the pressure signal is the same as that of the electrical signal. To simplify the model and simulate the vibration effect of PZT, the uniform vertical pressure load is applied on the top surface of excitation PZT to generate the guided-wave signal. The element types of the composite plate and PZTs are continuum shell (SC8R) and linear brick (C3D8R), respectively. The mesh size of the composite plate is 0.6 mm in thickness and 1 mm in other directions. The mesh size of PZTs are 0.5 mm. A dynamic explicit step with time 300 μs is created. After the model is solved, the in-plane stress in the thickness direction of the
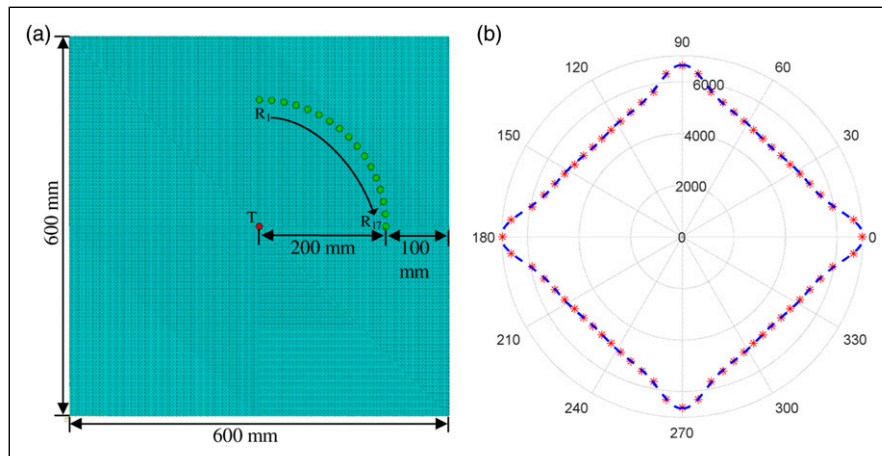
Figure 3. The simulation of velocity in all directions of CFRP. (a) The velocity model of CFRP. (b) Group velocity of CFRP in all directions.

PZTs center node is extracted to obtain the velocity. The starting time of the signal is determined by the intersection of the upper and lower envelope fitting lines, and is corrected by the auxiliary threshold 1×10^{-3}, which is introduced in detail in the following chapters. Then, the velocity of CFRP can be obtained by the 8-degree polynomial fitting. The calculated velocities are shown in Figure 3(b). This result is consistent with the stacking sequence of the CFRP plate, and has been verified in Ref 41. It can be found that the velocity in all directions appears like a diamond shape, and the velocity is the fastest when it is consistent with the fiber direction. In other words, the velocity of the guided wave is inversely proportional to the angle between wave direction and fiber direction. The velocity of the guided wave is 6969 m/s when it propagates along the 0° direction, that is parallel to the fiber direction. This value is close to the theoretical calculation as shown in Figure 2. The simulation results are reliable and can be used for NEPI of the composite plate.

Measurement of nonlinear parameter

The ability to detect small damage is very important to ensure structural health. Periodic nondestructive testing and on-line structural health monitoring can be used to track the occurrence and development of damage. The physical reason for the generation of nonlinear harmonics is that the acoustic wave interacts with the microstructure of materials, such as dislocation, crystal precipitation, fatigue crack, and early delamination damage. The sources of acoustic nonlinearity in solid media can be divided into two categories: classical nonlinearity and contact nonlinearity. The classical nonlinearity of solids is related to the anharmonicity of material lattice and crystal defects (e.g., dislocation and crystal precipitation), so it is also called the inherent physical nonlinearity of materials. Contact nonlinearity is caused by the existence of contact damage (e.g., closed crack and delamination damage), that is, there are contact interfaces. The nonlinearity of stress–strain relationship on the interface leads to the nonlinear distortion of ultrasonic guided wave. The nonlinearity of materials is closely related to the microstructure, which enables the nonlinear ultrasound to characterize the microstructure change of materials. In this paper, the nonlinear effect is observed to detect and characterize the contact delamination damage.

Compared with fundamental wave amplitude, material acoustic nonlinearity is a microwave quantity. The perturbation method is used to solve the problem. Consider the nonlinearity of the material, the one-dimensional Navier equation in the displacement field can be expressed as

$$\frac{\partial^2 u}{\partial t^2} - c^2 \frac{\partial^2 u}{\partial x^2} = c^2 \beta \frac{\partial u}{\partial x} \frac{\partial^2 u}{\partial x^2} \qquad (2)$$

where c is wave velocity, β is nonlinear parameter, and x is propagation distance. The simple harmonic solution of the wave equation is

$$\begin{aligned} u(x,\tau) &= A_1 \cos(\omega\tau) + A_2 \cos(2\omega\tau)x \\ &= A_1 \cos(\omega\tau) - \beta \frac{(A_1 k)^2}{8} \cos(2\omega\tau)x \end{aligned} \qquad (3)$$

where A_1 and A_2 are the amplitudes of fundamental and second harmonic waves, respectively, ω is angular frequency, and k is wave number. The nonlinear parameter β can be expressed as

$$\beta = \frac{8}{k^2 x} \cdot \frac{A_2}{A_1^2} \qquad (4)$$

It can be seen that the nonlinear parameter is directly related to wave number k, propagation distance k, and the amplitude ratio A_2/A_1^2. The wave number k is determined by fundamental frequency. Then, for a fixed propagation distance x, the nonlinear parameter is proportional to the amplitude ratio $\beta' = A_2/A_1^2$, which is known as the relative nonlinear parameter. The larger the value of β', the more obvious the distortion, and the more the energy transfer from fundamental frequency to higher harmonic. Therefore, the distortion caused by damage in the structure can be characterized by measuring nonlinear parameters.

Non-elliptical probability imaging method

Time coefficient. Similar to velocity, time information is an important factor for the accuracy of damage imaging. Especially for anisotropic composites, incorrect time information can lead to completely wrong damage detection result. As the difference between the damaged and pristine signal, scattered signal is the result of damage intervention. The head wave of the scattered signal can be used to obtain the arrival time after damage scattered. For isotropic materials, an ellipse with the excitation and recepting PZT as the focus can be determined according to the arrival time of the scattered signal, which is the path where damage may be in existence. Then, the damage can be localized and imaged in conjunction with multiple paths. However, for anisotropic composites, due to the different velocities in different directions, the elliptical probability imaging cannot be solved analytically in theory.[35] In this paper, the time difference of the arrival time between the scattered signal and the pristine signal is used for damage location. By comparing the time difference between the damage and reference point, the analytic solution process of the damage location is cleverly avoided. Since the damage determined by this method is located on a non-elliptical path, it is called non-elliptical probabilistic imaging.
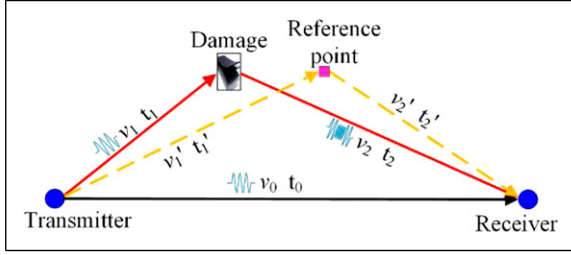
Figure 4. Schematic of damage location in an anisotropic composite plate.

Figure 4 shows the schematic of damage location in an anisotropic composite plate. In the figure, v_0, v_1, and v_2 are different due to anisotropy, so the damage location cannot be solved analytically. But, conversely, if the positions are known, the velocities can be obtained according to the simulation results. Therefore, the idea of reference point is introduced. For a given path, the positions of excitation, receiving, and reference points are determined, and the velocity between any two positions can be obtained according to the relative angles. The time difference $\Delta t = t_1 + t_2 - t_0$ of the signal received directly and after damage can be used to determine whether the reference point is on the damage path. Therefore, the time coefficient C_T is defined as

$$C_T = \frac{\Delta t' - \Delta t}{t_0} = \frac{(t_1' + t_2' - t_0') - (t_1 + t_2 - t_0)}{t_0} \quad (5)$$

The introduction of t_0 is to eliminate the influence of scale. When $\Delta t' - \Delta t = 0$, the reference point is located on the path determined by the damage. On the contrary, if the difference is larger, it means that the reference point is farther away from the damage path. Combined with multiple sensing paths, the damage location can be realized.

Time information is often obtained by threshold in most literatures. For the signal with less noise interference, such as simulation data, the threshold method is concise and accurate. However, when the data noise is large or the magnitude of the data differs greatly, the threshold method may lead to large errors. In this paper, the arrival time of pristine signal and scattered signal is needed for damage imaging. But the amplitude difference of pristine signal and scattered signal is large. Therefore, a new method is proposed to obtain the starting point of the signal according to the intersection of the data envelope fitting line. The signal is preprocessed by filtering and denoising, especially the experimental data. The maximum of the signal head wave is taken as the reference. The data between the low and high percentages of the maximum are taken for fitting. The intersection of the upper and lower envelope fitting lines can be used as the signal starting point.

As shown in Figure 5, the yellow dotted lines are the low and high percentages of the maximum. The magenta dash-dotted lines are the fitting lines of the upper and lower envelope. The blue "*" is the intersection point of the fitting lines, that is, the signal starting point. Compared with the threshold method, this method has better robustness, especially for the data with large noise or obvious zero drift. The first-order polynomial fitting method has better robustness, while the quadratic polynomial fitting method is more accurate. In addition, when the signal value is very small and there is no intersection point in the fitting curve or the slope is too small, the auxiliary threshold is used for correction.

Nonlinear damage index. The nonlinear ultrasonic guided wave detection method is highly sensitive to damage through the nonlinear effect caused by the interaction between acoustic wave and damage. The nonlinear component is essentially the energy leakage of the fundamental frequency linear component to higher harmonics. Therefore, the nonlinear component is very weak compared with the linear component, which brings difficulties to nonlinear feature extraction. On the other hand, the propagation distance of different paths is different. The nonlinear component of the received signal also contains other
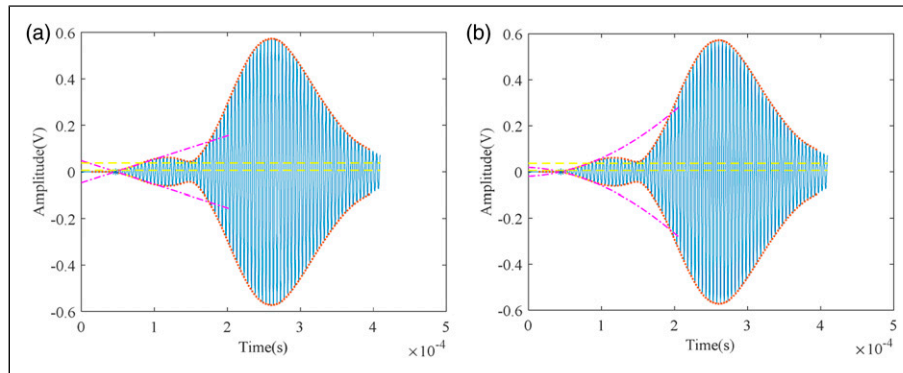

Figure 5. Starting time based on data envelopment fitting. (c) First-order polynomial fitting. (d) Quadratic polynomial fitting.

nonlinear components in addition to the part affected by the damage. But, for the same path, the difference in the nonlinear component of the received signal is caused by damage. Therefore, the damage is characterized by the nonlinear features' difference between damaged and pristine signals in this paper. The preprocessed signal is further normalized to eliminate the dimension of the signal and improve the robustness. The smooth pseudo Wigner–Ville distribution (SPWVD) has good time–frequency concentration, time–frequency edge characteristics, and cross-term suppression ability. To obtain accurate frequency information, SPWVD is adopted. The expression of SPWVD is

$$
\begin{aligned}
&SPWVD_x(\omega,t)\\
&= \iint g(u)h(\tau)x\left(t-u+\frac{\tau}{2}\right)x^*\left(t-u-\frac{\tau}{2}\right)e^{-j2\pi\omega\tau}\mathrm{d}u\mathrm{d}t
\end{aligned}
\tag{6}
$$

where $g(u)$ and $h(\tau)$ are time window function and frequency-domain window function, $x(t)$ is input signal, and $x^*(t)$ is its conjugate. The time–frequency information of the signal can be obtained by SPWVD. According to the equation (4), the energy of fundamental and second harmonic components are used to calculate the nonlinear feature. Therefore, the nonlinear coefficient (NC) is calculated by

$$
NC = \frac{\sum_{k=1}^{N} E_{2\omega}(k) - \sum_{k=1}^{N} E_{\omega}(k)}{\left[\sum_{k=1}^{N} E_{\omega}(k)\right]^2}
\tag{7}
$$

where k is discrete data points, N is the integral data length, $E_{2\omega}(k)$ and $E_{\omega}(k)$ are energy spectrum of fundamental and second harmonic, respectively. Ulteriorly, the nonlinear damage index (NDI) based on NC is defined as

NCD- NCB
$$
NDI = \frac{(NC_D - NC_D)_{if<0,0}}{NC_B}
\tag{8}
$$

where NC_D and NC_B are the nonlinear coefficients of damaged and pristine signals. $if<0,0$ means if the value is less than 0, set to 0.

Damage probability imaging. Time coefficient C_T is used to determine the damage path, and the NDI is used to determine the value of damage probability. By accumulating the probability values of multiple paths, damage location and imaging can be realized. Therefore, the damage probability is defined as

$$
P(x,y) = \sum_{n=1}^{N_P} p_n(x,y) = \sum_{n=1}^{N_P} NDI_n \cdot H_n(x,y)
\tag{9}
$$

where $p_n(x,y)$ is the estimated probability value of the n_{th} path. N_P is the total number of excitation-receiving paths. $H_n(x,y)$ is the scaling control function related to C_T

$$
H_n(x,y) = \begin{cases} 1 - \dfrac{1}{\gamma}.C_T, & C_T < \gamma \\ \\ 0, & C_T \geq \gamma \end{cases}
\tag{10}
$$

where γ is a scaling coefficient controlling the decay rate of the probability value, and is inversely proportional to it. To further quantify the imaging quality, a damage probability energy ratio based on image energy is defined

$$
E_r = \frac{\sum\limits_{x'_M,y'_M \in D} [P(x'_M,y'_M)]^2}{\sum\limits_{x_M,y_M \in A} [P(x_M,y_M)]^2}
\tag{11}
$$

where D is the damage area set, and A is imaging area set. The larger the damage probability energy ratio E_r, the better the imaging effect.

The damage information of the composite plates can be obtained by displaying the cumulative probability of all paths with image. Figure 6 shows the specific process of the NEPI method.
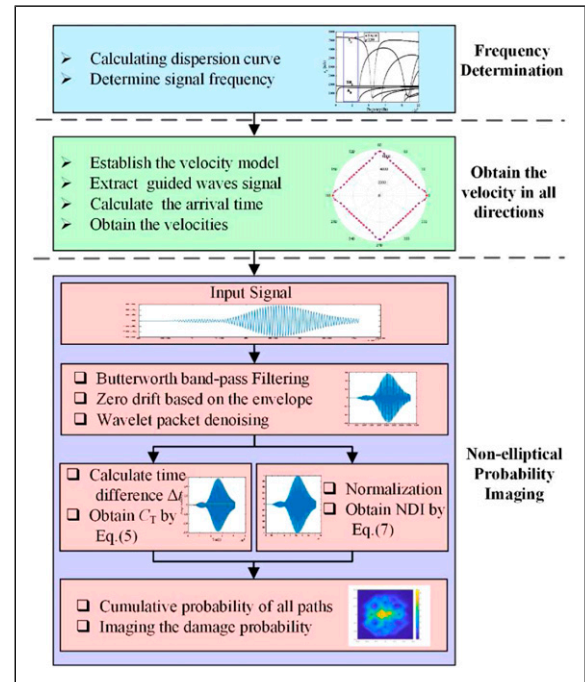

Figure 6. Flowchart of the velocity anisotropy probability imaging method.

Numerical simulation

The finite element model is performed to simulate the interaction between the ultrasonic guided waves and delamination. The delamination model of a CFRP composite plate is shown in Figure 7. In the surface of the composite plate, 8 PZTs are symmetrically arranged on a circle with 150 mm radius. The delamination damage is parallel to the surface of the composite plate. It is located at 1/5 of the thickness, and a quarter radius away from the center of the circle. The material parameters and sizes of composite plate and PZTs are consistent with those in the velocity simulation model. Separate faces are cut in the delamination area to get two independent surfaces for setting the contact pair. The remaining cutting faces are constrained by "Tie". A "surface-to-surface contact" with size 15 × 30 mm is set to simulate the contact delamination damage. The "normal behavior" and the "tangential behavior" are set to "hard contact" and "penalty with 0.3 friction coefficient". An undamaged model is also established for comparative analysis. The only difference between the damaged and undamaged model is the existence of contact delamination. Because the nonlinear characteristics are obtained from the frequency domain, a 50-peak sine wave with a frequency of 200 kHz and modulated by the Hanning window is adopted to generate a sufficiently strong and energy-intensive guided-wave signal. All PZTs are excited in turn, and the in-plane stress is extracted as the received signal.

Figure 8 shows the received simulation signal of PZTs when PZT 5 is used as excitation. It can be seen that the amplitude difference between the pristine signal and the scattered signal is large. Especially in the initial part of
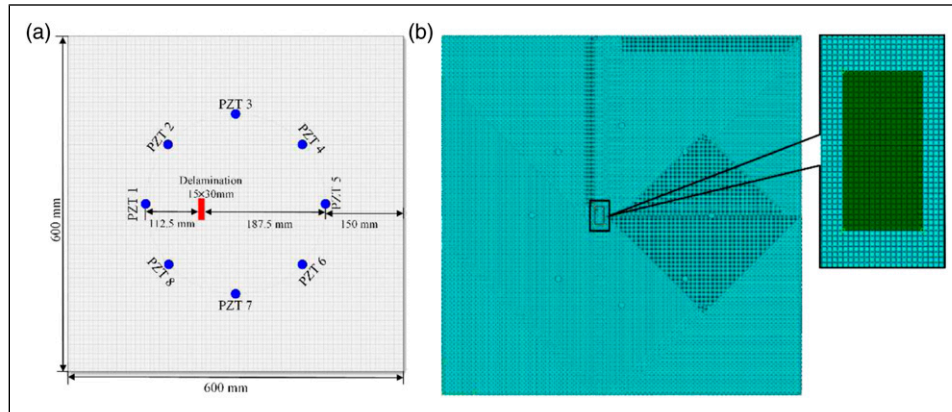

Figure 7. The delamination model of a CFRP composite plate. (a) Schematic of damage and PZT distribution. (b) The mesh model with delamination.
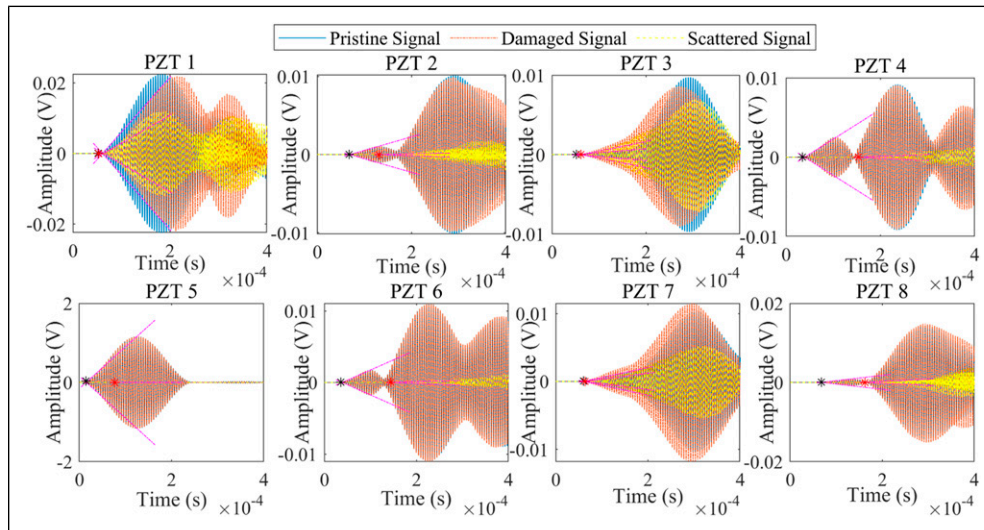

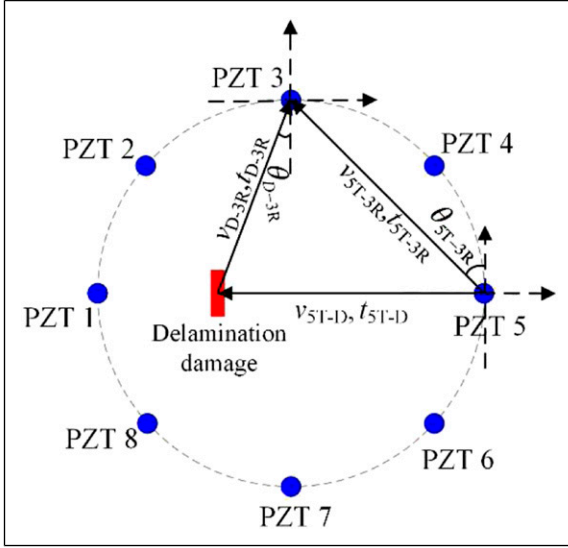**Figure 8.** Simulation signal of PZTs when PZT 5 as excitation.

Figure 9. Schematic of guided-wave propagation.

the scattered signal, the amplitude is very small, which means the threshold method may lead to errors. The blue line, orange dot-dashed line, and yellow dashed line represents the pristine, damaged, and scattered signals. The magenta dash-dotted line is the envelope fitting line, and its

intersection point is the signal starting point, as shown by the asterisk "*" in the figure. PZT 5 is the excitation, which is least affected by delamination damage. Since the delamination is located on the path 5T-1R (iT-jR means path that PZT i is excitation and PZT j is receiving), the received signal of PZT 1 is most affected by the damage. Figure 9 shows the schematic of guided-wave propagation. θ_{iT-jR} means the minimum angle between the path iT-jR and the fiber direction. Similarly, θ_{D-jR} means the minimum angle between the path D-jR and the fiber direction, and D is the damage. The angle θ_{5T-D} is equal to zero, and the angle θ_{D-3R} and θ_{D-7R} is smaller than θ_{5T-3R}. Therefore, the velocities v_{5T-D}, v_{D-3R} ,and v_{D-7R} are faster than v_{5T-3R}. From Figures 8 and 9, the propagation time of the guided wave arriving at PZT 3 and PZT 7 through the damage is only a little longer than that of the direct wave. The received signals of PZT 3 and PZT 7 are more affected by the damage. The received signals of remaining PZTs are less affected by the damage. It can be seen that the smaller the angle between PZT and the damage, the more vulnerable it is to damage.

Furthermore, the time-frequency analysis of the signal is performed. Take path 5T-1R as an example, the time-frequency result of fast Fourier transform (FFT) and SPWVD are shown in Figure 10. Figure 10(a) shows the
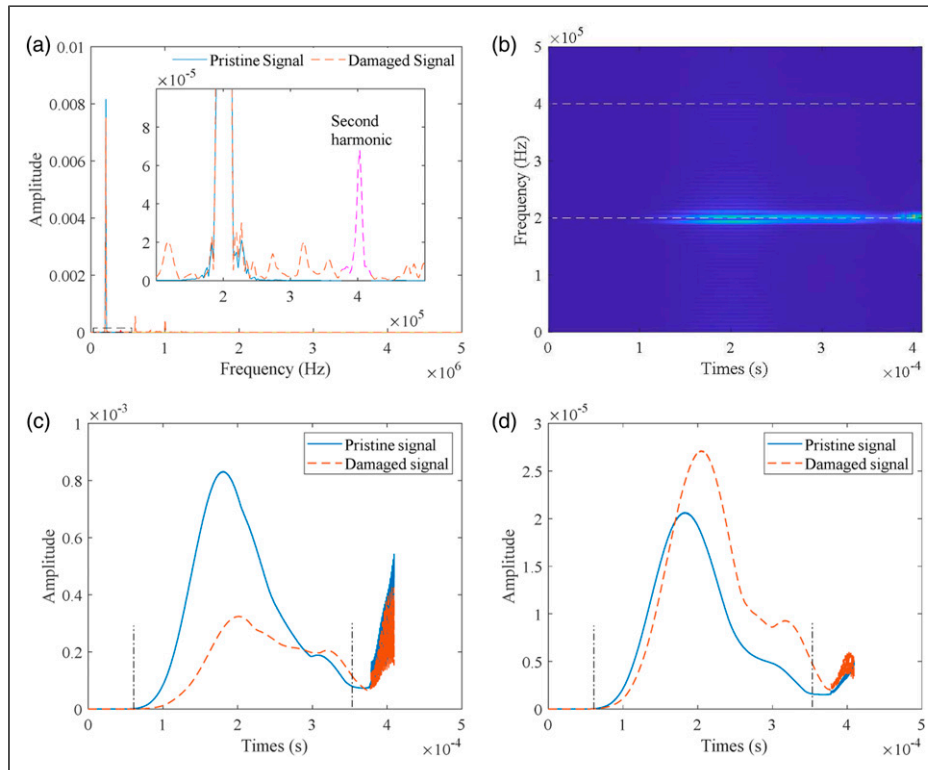

Figure 10. Time-frequency analysis of path 5T-1R. (a) Fast Fourier transform results of pristine and damaged signal. (b) SPWVD time-frequency diagram of damaged signal. (c) Amplitude profiles of fundamental frequency after SPWVD. (d) Amplitude profiles of second harmonic after SPWVD. SPWVD: smooth pseudo Wigner–Ville distribution.

FFT results of pristine and damaged signal. The signal energy concentrates on the fundamental frequency component. After amplification, it can be seen that compared with the pristine signal, the energy of the damaged signal is partly transferred from the fundamental frequency component to the multiple-frequency component. Figure 10(b) shows the SPWVD time-frequency diagram of damaged signal. It can also be seen that the energy is concentrated in the fundamental frequency component. The second harmonic component is almost invisible, which also reflects the weak of nonlinear features. Figure 10(c) and (d) show the amplitude profiles of fundamental frequency and second harmonic through SPWVD, which more clearly show the amplitude changes of fundamental frequency and second harmonic. The second harmonic amplitude of the damaged signal is significantly greater than that of the pristine signal, while the fundamental frequency amplitude of the damaged signal is significantly less than that of the pristine signal. This is consistent with the result of FFT as shown in Figure 10(a).

Due to the end effect and multimodal interference, the received signal is very complex. Figure 2 shows that the velocity of the S_0 mode is the fastest, which means that the interference of the S_0 mode is the least in a short time from receiving the signal. Therefore, to reduce the interference of other guided-wave modes, the data of head wave with a certain length is taken for feature extraction and analysis. In this paper, 3000 data points of head wave, that is, the data points between the two dash-dotted lines in Figure 10, from the starting point are intercepted to calculate the nonlinear coefficient. The starting point of the signal is the intersection of the upper and lower envelope fitting lines, as shown in Figure 8. According to equation (8), the NDI of all paths is calculated. To verify the effectiveness of NDI, the damage index of scattered signal (SDI) is defined. As the difference between the damage signal and the pristine signal, the scattered signal can be used to characterize the effect of damage

intervention to a certain extent. Therefore, the SDI is calculated by the following formula

$$SDI = \frac{\sum_{k=1}^{N} [S_D(k) - S_B(k)]^2}{\sum_{k=1}^{N} [S_B(k)]^2} \qquad (12)$$

where $S_B(k)$ and $S_D(k)$ are pristine and damaged signal, respectively. N is the data length.

To reduce the difference caused by different PZT as excitation, the normalization is performed. Figure 11 shows the normalized damage feature of all paths. In a combination of Figures 8, 9, and 11, it can be seen that the impact of damage on PZT 1, 3, 5, and 7 is relatively large. This is because the damage is located on the path formed by PZT 1 and PZT 5, and the angle θ_{D-3R} and θ_{D-7R} is small. Among them, the damage index of PZT 1 as receiving transducer is relatively large, since the distance between PZT 1 and damage was the shortest. The NDI of the path 2T-6R and 4T-8R are larger because the distance between the damage and the path is very small. Both NDI and SDI describe these characteristics accurately on the whole, but there are some differences. For example, when PZT 5 is the excitation, the NDI of path 5T-1R is the largest, while the SDI of path 5T-3R is the largest, followed by 5T-1R. When PZT 3 or PZT 7 are excitation transducers, the NDI is the maximum when PZT 1 is used as the receiving transducer, and the SDI are the maximum in path 3T-7R and 7T-3R, respectively.

The first-order envelope fitting with an auxiliary threshold of 3×10^{-5} is adopted to obtain the time difference Δt, which shows good robustness. The time difference Δt of all paths is shown in Table 2. When the excitation and receiving PZT are the same PZT, its time difference is set to 0. Because the fitting curve slope of the scattered signal is usually smaller than that of the pristine signal, Δt will be negative in a few cases, resulting in errors. Therefore, if the time difference is negative, it is set to 0. Again, since the
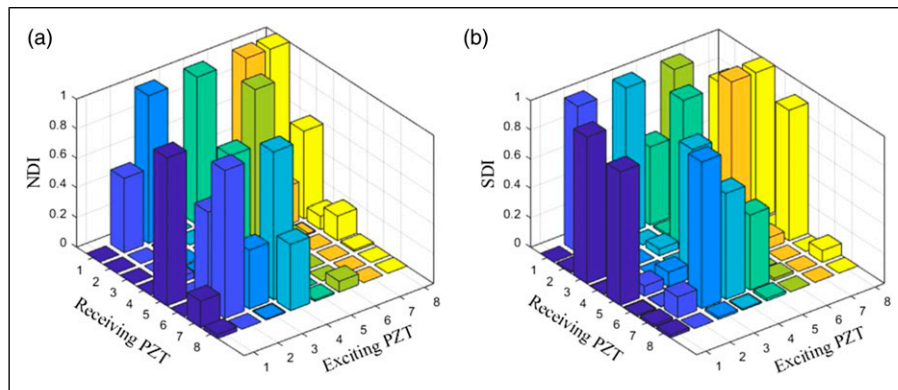

Figure 11. Normalized damage index of all paths. (a) NDI of smooth pseudo Wigner–Ville distribution. (b) SDI.

Table 2. Time difference Δt of all paths, T and R represent the excitation and receiving PZT.

Δt (10^{-5}s)	1T	2T	3T	4T	5T	6T	7T	8T
1	0	0	0	0	0.16	1.62	1.23	0.90
2	8.48	0	10.6	11.2	6.37	10.5	3.25	11.5
3	6.90	0.41	0	0.24	0.96	1.29	0.10	0.17
4	5.34	11.9	9.67	0	11.8	14.8	6.95	10.0
5	0.13	0.26	0.45	0.22	0	0.19	0.40	0.11
6	4.33	9.88	6.69	14.6	10.9	0	11.8	11.9
7	2.00	1.29	0.10	0.16	0.36	0.41	0	0.24
8	6.75	10.5	3.88	11.7	9.46	13.7	8.94	0

damage is located on the path formed by PZT 1 and PZT 5, and the angle between the damage and PZT 3 or PZT 7 is small, Δt is relatively short when PZT 1, 3, 5, and 7 are receiving transducers. When the path is consistent with the fiber direction (e.g., paths 2T-4R, 2T-8R, 4T-2R, 4T-6R, 6T-4R, and 6T-8R), the velocity of guided wave is faster, and the time difference after damage is relatively large.

According to equation (5), the time coefficient C_T between the reference point and damage can be calculated. Then, the damage imaging can be realized by combining the damage feature. The results of NEPI with different PZT as excitation are shown in Figure 12. PZT iT means the damage imaging obtained when PZT i is used as the excitation and other PZTs as the receiving. The scaling coefficient γ is set to 0.5. It is worth noting that when the value of γ is smaller, the probability decays faster, and the accuracy requirements for Δt are higher. On the contrary, the greater the value of γ, the lower the accuracy requirements for Δt. When PZT 1, 3, 5, and 6 are used as excitation, the NDI imaging shows accurate damage location imaging results. When PZT 4 and 7 are used as excitation, the imaging results deviate a little from the damage. When PZT 2 and 8 are used as excitation, the imaging results do not accurately show the damage location. The SDI imaging can also show the damage location when some PZT are used as excitation, but on the whole, it is not as accurate as the NDI imaging.

The velocity is the fastest along the fiber direction and the smallest along the 45° direction, which presents
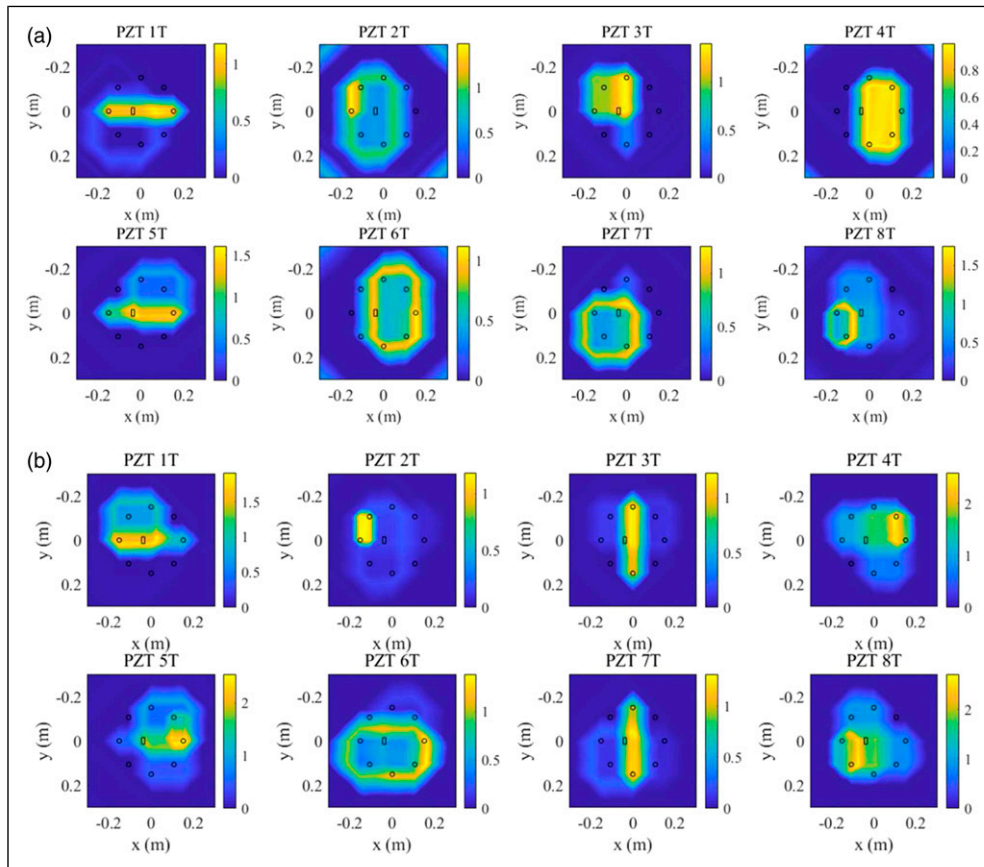
Figure 12. Non-elliptical probability imaging with different PZT as excitation. (a) NDI imaging result with different PZT as excitation. (b) SDI imaging result with different PZT as excitation.
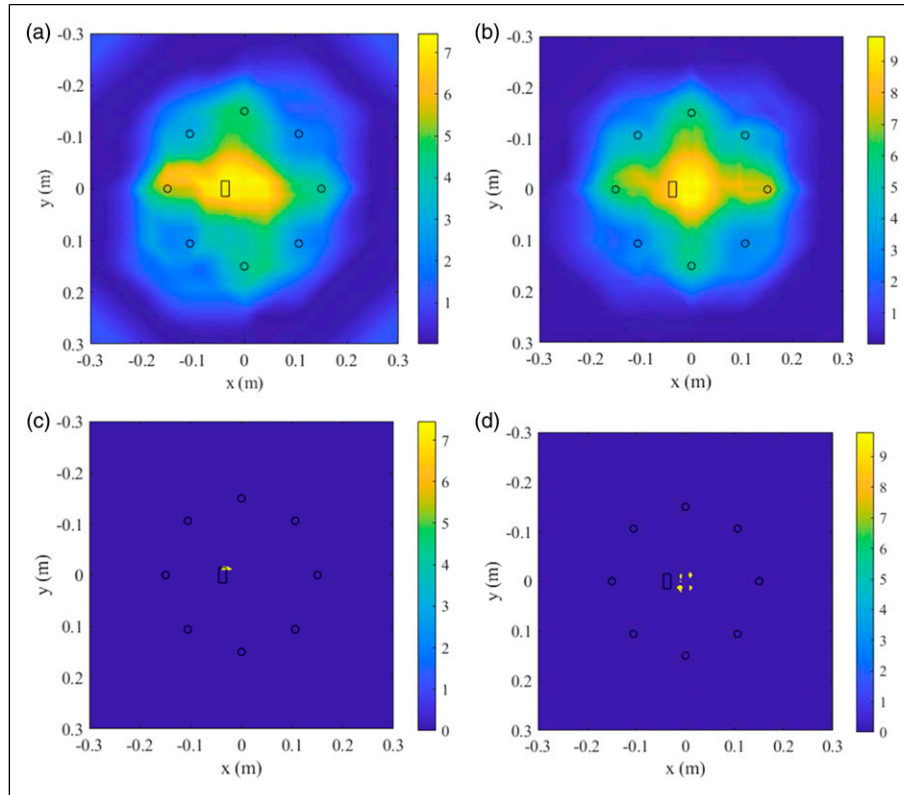
Figure 13. Non-elliptical probability imaging using all paths. (a) NDI imaging result using all paths. (b) SDI imaging result using all paths. (c) NDI imaging result using all paths by applying a threshold of 99%. (d) SDI imaging result using all paths by applying a threshold of 99%.

an irregular shape. This is also the reason why this method is called non-elliptical probability imaging. Therefore, no matter where the reference point is located in the rectangle formed based on the excitation, reception, and fiber direction, the arrival time after the damage is only a little longer than that of the direct wave. This is not conducive to the detection of damage in the rectangle, but it can be compensated by probability accumulation of all paths.

Figure 13 shows the results of NEPI using all paths. In the NDI imaging, the damage is in the brightest region, while in the SDI imaging, the damage is in the edge of the brightest region. According to equation (11), the damage probability energy ratio E_r is calculated to evaluate the imaging quality. The E_r of NDI imaging is 1.33%, and that of SDI imaging is 1.22%. Because the damage area is much smaller than the whole imaging area, the value of E_r is small. The damage probability of NDI imaging is more concentrated on the damage location than SDI imaging. By applying the 99% threshold, the damage imaging effect can be seen more clearly. In the NDI imaging, most of the damage is still located in the highlighted area, and the value of E_r is increased to 53.86%, while in the SDI imaging, the damage is completely outside the highlighted area, and the value of E_r is 0. The non-elliptical probability

imaging based on the nonlinear ultrasonic guided wave can identify the damage and accurately present the damage location.

Experimental results and discussions

Experimental platform

Following the numerical simulation, the proposed NEPI is verified by artificially simulated delamination damage on an anisotropic CFRP plate. The schematic of the experimental platform is shown in Figure 14. The experiment was carried out in an air-conditioned room with a temperature of 26°C. The experimental environment temperature is relatively stable, and the temperature effects are not considered in this paper. The material parameters and dimensions of CFRP plate and PZTs are consistent with those in simulation. The positions of PZTs and delamination damage are also consistent with the simulation. The center frequency of PZTs is 2 MHz. Due to the different velocities and attenuation rates of the anisotropic CFRP structure in different directions, the guided wave in the anisotropic CFRP plate is very complex. On the other hand, the nonlinear ultrasonic guided waves are highly sensitive to damage and are susceptible to interference. Therefore, the experimental conditions should be

Figure 14. The schematic of the experimental platform.

kept consistent to accurately measure the nonlinearity caused by contact damage. It is difficult for realistic delamination damage because it is inside the structure. To simulate contact delamination damage more truly, half the area of the mass block is attached to the composite plate with a coupling agent. In this way, two incompletely separated surfaces are generated, which is similar to contact delamination damage. The coating area of the coupling agent (Dow Corning HVG, Midland, MI, USA) is 15 × 30 mm, which is also consistent with the simulation. The weight of the mass block is 706 g, and the size is 25 mm × 30 mm × 120 mm.

To obtain better frequency domain information, a 200-kHz 50-peak sine wave with 6V (Vp-p) modulated by the Hanning window is generated by the function generator (Agilent 33522B, Palo Alto, Santa Clara County, CA,

USA). The amplifier (TREK2100HF, Trek Inc., New York, NY, USA) with 50 times the stable amplification is used to amplify the generated guided-wave signal. The acquisition device was composed of four 4-channel high-speed data acquisition cards (TDEC PCI-20614, Chengdu, CN) with a sampling rate of 25 MHz and PC, which fully meets the requirements of signal collection. The sampling rate in the experiment is 10 MHz.

Experimental results and analysis

The simulation signal mainly depends on theoretical calculation, while the experimental signal is collected by experimental devices and instruments, which is more vulnerable to noise interference. The preprocessing progress, including filtering, zero-drift removal, and wavelet packet denoising, is performed. The Butterworth band-pass filter is applied, and stopband and passband cutoff frequency are 100 and 500 kHz. The zero drift is reduced by subtracting half of the difference between the absolute value of upper and lower envelope. Then, three-layer wavelet packet decomposition is carried out, and the wavelet packet coefficients including fundamental frequency and second harmonic components are extracted to reconstruct the signal.

The starting time of the signal is also obtained by the first-order envelope fitting. Because of the different dimensions of signals, the auxiliary threshold is set to 3×10^{-3}. When PZT 5 is used as the excitation, the experimental received signal is shown in Figure 15. The blue line, orange dot-dashed line, and yellow dashed line represents the pristine, damaged, and scattered signals. The arrival time of path 5T-1R (along the 0° direction) is 7228.9 m/s, which is close to the value of dispersion curve

Figure 15. Experimental signal of PZTs when PZT 5 as excitation.

and velocity simulation. This shows the reliability of the simulation. There is little difference between damaged and pristine signal in wave packet shape and mode, and the difference is mainly reflected in amplitude. This is similar to the simulation results shown in Figure 8. The received signal of PZT 1 has a significant decrease in amplitude because the damage is located on path 5T-1R. The received signal amplitude of PZT 2 and PZT 8 decreases slightly. The received signals of other PZTs are less affected by the damage, and the difference between damaged pristine signal is small. The difference between the damage signal and the pristine signal of PZT 3 and 7 was not reflected when PZT 5 is the excitation.

The experimental time-frequency analysis of path 5T-1R is shown in Figure 16. Similar to the simulation, the fundamental frequency amplitude of the pristine signal is obviously larger than that of the damaged signal. The FFT results of experimental data are noisier than those of simulation. The amplitude profiles of fundamental frequency and second harmonic are shown in Figure 16(c) and (d). The second harmonic amplitude of the pristine signal is still larger than the damaged signal. But the proportion of the second harmonic is obviously increased, which also means that the nonlinear coefficient increases. In other words, the existence of damage leads to the increase of nonlinear component.

The experimental NDI of all paths based on SPWVD is calculated with 3000 data points of head wave, as shown in Figure 17. Similar to the simulation results, the NDI of most signals received by PZT 1, 5, 3, and 7 has more obvious nonlinear effects because the damage is located on the path formed by PZT 1 and PZT 5, and the angles θ_{D-3R} and θ_{D-7R} are smaller. The value of NDI is relatively lower in paths 2T-6R, 4T-8R, and its inverse paths when these paths are close to the damage. The reason for this result is that the angles between these sensor paths and the fiber direction are the largest. The nonlinear feature can easily be buried in the noise. On the other hand, the amplitude of nonlinear feature is small, which means it is easy to fluctuate, especially for experimental data. The value of NDI is relatively high in paths 2T-4R, 2T-8R, 4T-2R, and 6T-8R because the angles between the sensor path and fiber direction are 0. Similarly, the two PZTs which are close to each other have high speed and short distance, and the corresponding signal strength is generally large, for example, 3T-4R, 4T-5R, 7T-8R, and so on. On the whole, the nonlinear features can reflect the damage state.

The NEPI considers the anisotropic velocity on the basis of EPI. In fact, EPI is a special case of NEPI. Therefore,
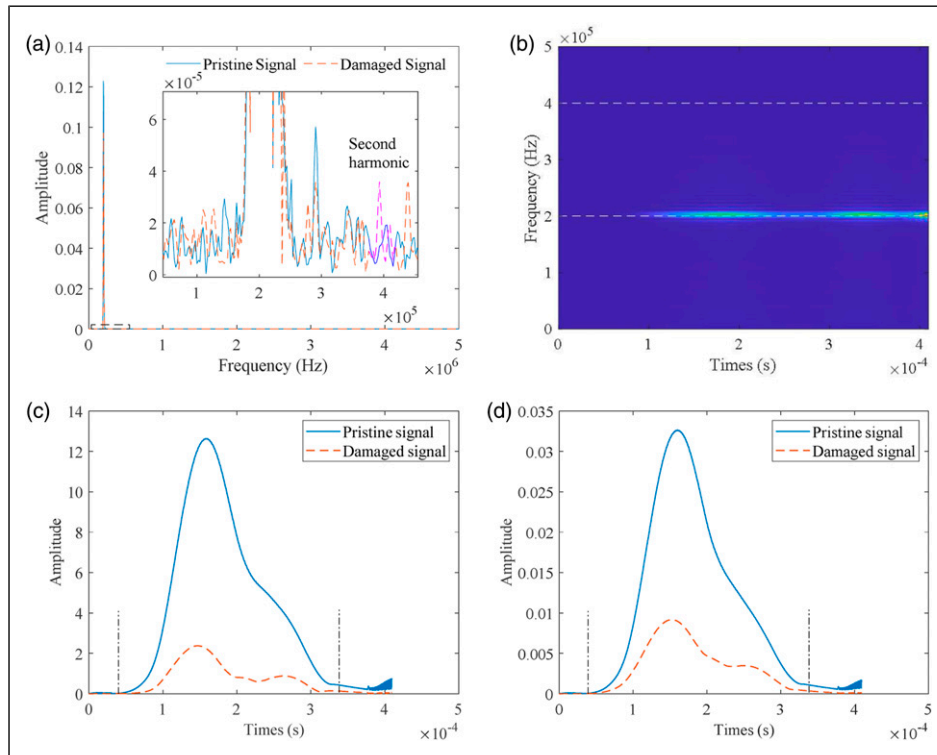

Figure 16. Experimental time-frequency analysis of path 5T-1R. (a) Fast Fourier transform results of pristine and damaged signal. (b) SPWVD time-frequency diagram of damaged signal. (c) Amplitude profiles of fundamental frequency after SPWVD. (d) Amplitude profiles of second harmonic after SPWVD. SPWVD: smooth pseudo Wigner–Ville distribution
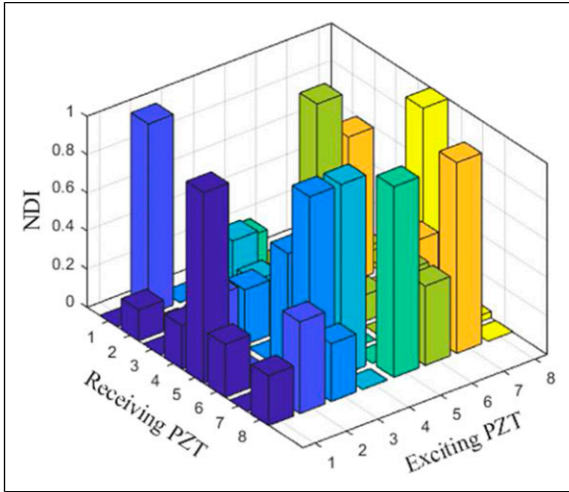
Figure 17. Experimental NDI of all paths based on smooth pseudo Wigner–Ville distribution.

NEPI and EPI were performed and compared. Figure 18 shows the experimental results of damage probability imaging with different PZT as excitation. Figure 18(b) shows the result of EPI, and the velocity is the same and set to

5935 m/s (the mean value of the lowest and highest velocity). The scaling coefficient γ is also set to 0.5. From Figure 18(a), when PZT 1, 3, 4, 7, and 8 are used as excitation, the NDI imaging shows good imaging results. It can be seen that the damage path determined by the NEPI method is an irregular non-elliptical path, while the damage path determined by the EPI method is an elliptic path. When a single PZT is used as the excitation, sometimes it can show an ideal damage imaging effect, but sometimes the imaging effect is not good. This is also the advantage of multipath superposition, which can improve the robustness of NEPI. There is a certain deviation in the highlighted area of damage imaging compared with NEPI, for example, the results when PZT 3, 4, and 7 are used as excitation.

Further, the probability of all paths is superimposed and imaged to obtain the nonlinear feature damage imaging results as shown in Figure 19. In Figure 19(a), the actual damage position of NEPI imaging is almost in the center of the brightest region, which reflects the accuracy of the NEPI method for the anisotropic composite plates. In Figure 19(b), the damage probability of EPI imaging that should be concentrated at the damage is dispersed since the anisotropy is not considered. The damage probability
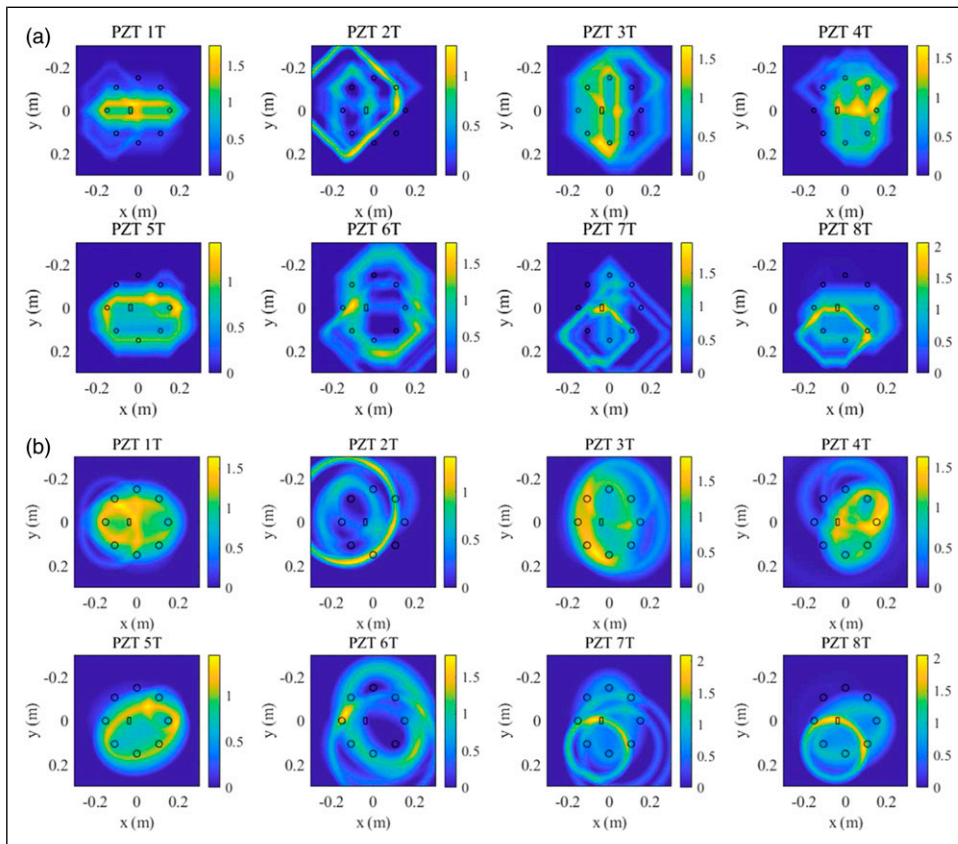

Figure 18. Damage probability imaging of experimental data using NDI with different PZT as excitation. (a) Non-elliptical probability imaging results with different PZT as excitation. (b) EPI results with different PZT as excitation.
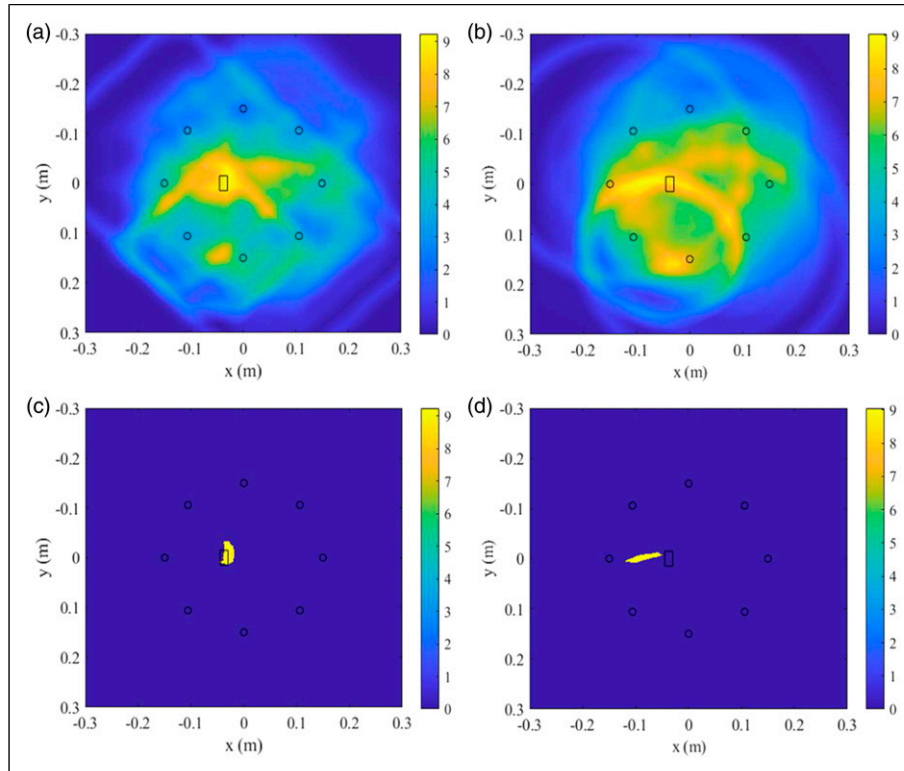
Figure 19. Damage probability imaging of experimental data using NDI of all paths. (a) NEPI result using all paths. (b) EPI result using all paths. (c) NEPI result using all paths by applying a threshold of 96%. (d) EPI result using all paths by applying a threshold of 96%. NEPI: non-elliptical probability imaging.

energy ratio E_r of NEPI imaging is 1.18%, and that of EPI imaging is 0.73%. When the threshold value of 96% is applied, the damage imaging results are more intuitive and clear. Most of the actual damage of NEPI imaging is still in the bright region and the value of E_r is increased to 33.54%, while the actual damage of EPI imaging is almost entirely outside the bright area. The non-elliptical probability imaging based on the nonlinear ultrasonic guided wave shows a good location and detection ability to delamination damage.

Method comparisons

Comparison of crack damage imaging based on SDI. The crack damage is perpendicular to the structure surface, which divides the structure into two parts and blocks the propagation of guided waves.[42,43] The delamination damage is parallel to the structure surface, and the blocking effect on the sound wave in the propagation direction is limited. Linear characteristics such as scattered signal have a good detection effect on crack damage. Therefore, the scattered signal is used to detect the crack and delamination damage, respectively, to verify the micro damage sensitivity of the nonlinear feature. A crack damage experiment of

anisotropic composite plates with the same size is carried out to further verify the detection ability of the nonlinear feature. In the crack experiment, a 200-kHz, 5-peak sine wave modulated by the Hanning window was excited to make the signal energy more concentrated. 16 PZTs are used and evenly arranged on the circle with radius of 300 mm. The size of crack damage is 10 mm in width. The location of crack damage is the same with the delamination experiment. The material parameters of the composite plate, PZT, and other experimental parameters are consistent with the delamination experiment.

The obtained non-elliptical probability imaging results of crack and delamination experiments using SDI are shown in Figure 20. The crack damage is completely contained in the bright region of the imaging results. However, the imaging results of delamination damage are inaccurate, and the damage is almost outside the bright region. After 96% threshold was applied, the results were more obvious. The accurate imaging of crack damage shows the effectiveness of SDI. However, delamination damage, especially early delamination damage, is difficult to effectively reflect the acoustic wave because it is small and parallel to the structure surface, which makes it difficult to detect. The scattered signal of delamination is not as obvious as that of crack
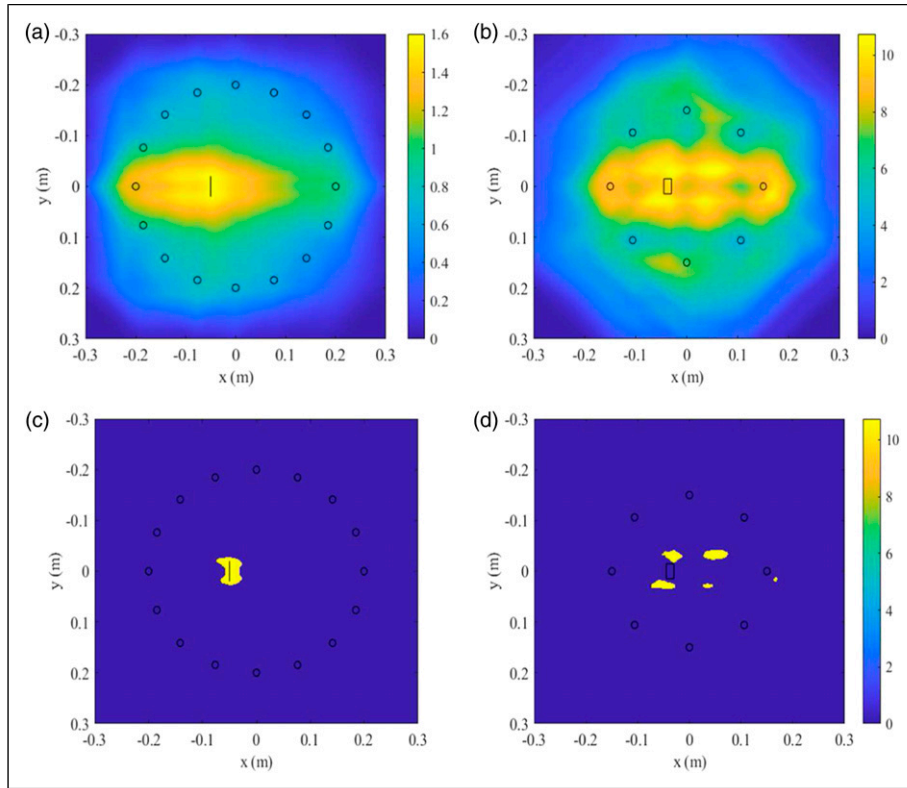
Figure 20. Non-elliptical probability imaging of experimental data using SDI. (a) SDI imaging of crack damage. (b) SDI imaging of delamination damage. (c) SDI imaging of crack damage by applying a threshold of 96%. (d) SDI imaging of delamination damage by applying a threshold of 96%.

damage. The smaller scattered signal also makes it difficult to obtain the time coefficient, which is one of the reasons for using envelope fitting to obtain the arrival time. While the SDI cannot accurately describe the delamination damage information, the nonlinear feature accurately describes, as described in the previous section. The detection ability of nonlinear features for delamination damage is verified by comparing the scattered signal with the crack and delamination damage.

Comparison of nonlinear feature. Nonlinear features are mainly extracted from the frequency domain of the signal. Three common frequency or time-frequency analysis methods including FFT, short-time Fourier transform (STFT), and S-transform (ST) are used to extract the NDI and compare with SPWVD. The NDI of FFT is calculated by dividing the second harmonic by the square of the fundamental amplitude. The NDI of STFT and ST are consistent with the calculation method of SPWVD. After
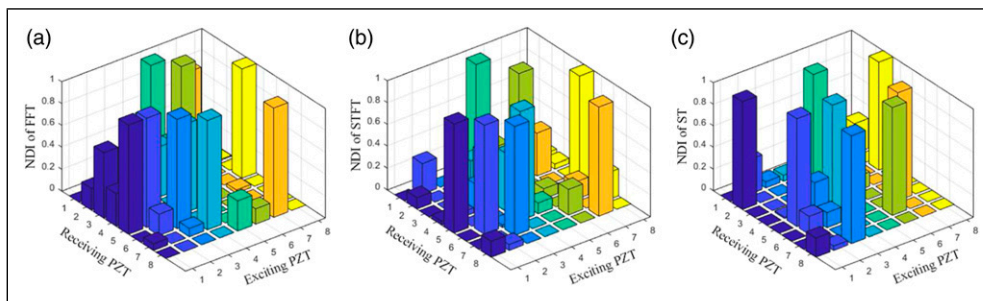

Figure 21. NDI obtained by different method. (a) NDI obtained by fast Fourier transform. (b) NDI obtained by short-time Fourier transform. (c) NDI obtained by S-transform.
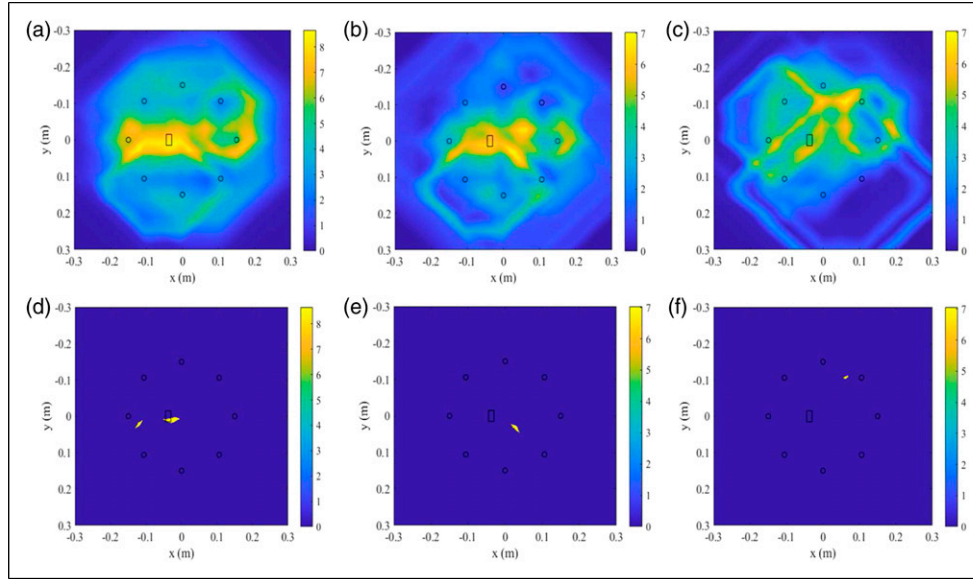
Figure 22. Non-elliptical probability imaging results of different method. (a) NEPI result of FFT. (b) NEPI result of STFT. (c) NEPI result of ST. (d) NEPI result of FFT by applying a threshold of 96%. (e) NEPI result of STFT by applying a threshold of 96%. (f) NEPI result of ST by applying a threshold of 96%. NEPI: non-elliptical probability imaging; STFT: short-time Fourier transform; FFT: fast Fourier transform; ST: S-transform.

extracting the second harmonic and fundamental components, the NDI of STFT and ST are calculated according to equations (7) and (8). The NDI of different method is shown in Figure 21. NDI of FFT and STFT in paths 1T-5R, 3T-7R, and their inverse paths are large which is similar with SPWVD. The NDI of FFT and STFT in some paths is different from that of SPWVD, but the overall trend is consistent. However, NDI of ST in paths 1T-5R, 3T-7R, and their inverse paths are small. Moreover, the NDI of ST is larger in the partially receiving PZT adjacent to the excitation, which brings interference to the damage imaging.

Then, the NDI of FFT, STFT, and ST are applied to the NEPI as shown in Figure 22. The NDI of FFT locates the damage relatively accurately, and it is clearer after applying 96% threshold, but there are some artifacts. The damage imaging using the NDI of STFT is also bright in the damage location, that is, the damage probability is high, but the brightest area is not the actual damage location. The damage imaging using the NDI of ST shows the wrong damage location. This is consistent with the result presented by the NDI of ST. Obviously, compared with these three methods, SPWVD can extract time-frequency features more accurately. Because the nonlinear component is generated by the interaction between the guided wave and damage, the nonlinear component is very small compared with the fundamental component. This makes the extraction of nonlinear features more difficult. The SPWVD has high time-frequency resolution, which is conductive to the

extraction of nonlinear feature. The imaging results also show that SPWVD can present the damage location more accurately.

Conclusions

In this paper, aiming at the contact delamination damage detection of anisotropic composite plates, a NEPI method based on nonlinear ultrasonic guided waves is proposed. The anisotropic characteristics of the composite plate are analyzed theoretically, and detection frequency is determined. Then, the velocities in all directions of the composite plate are obtained by the finite element simulation technology. The time coefficient C_T based on the time difference Δt is defined. By comparing the C_T of damage with that of the reference point, the problem that the damage location cannot be solved analytically is avoided skillfully. Furthermore, the intersection of the upper and lower envelope fitting lines is used to improve the way to get start time. The nonlinear damage index (NDI) is used to characterize the delamination damage, and both simulation and experiment verify its effectiveness as a damage index. The sensitivity of NDI to delamination damage is further verified by comparing with the crack damage imaging based on SDI. The reliability of the NDI extraction method based on SPWVD is demonstrated by comparing with FFT, STFT, and ST.

In conclusion, the proposed NEPI method based on nonlinear ultrasonic guided waves can detect the delamination damage with good location accuracy and high damage sensitivity. The introduction of nonlinear features

greatly improves the detection ability of the method for delamination damage. The next research can be carried out around the detection of multiple damage conditions, and the distribution of sensors can be optimized to enhance the application value.

Declaration of conflicting interests

The author(s) declared no potential conflicts of interest with respect to the research, authorship, and/or publication of this article.

Funding

ORCID iDs

Xiaobin Hong https://orcid.org/0000-0002-2392-2556
Bin Zhang https://orcid.org/0000-0002-6912-7953

References

1. Marcantonio V, Monarca D, Colantoni A, et al. Ultrasonic waves for materials evaluation in fatigue, thermal and corrosion damage: A review. *Mech Syst Signal Process* 2019; 120: 32–42.

2. Mardanshahi A, Nasir V, Kazemirad S, et al. Detection and classification of matrix cracking in laminated composites using guided wave propagation and artificial neural networks. *Compos Structures* 2020; 246; 112403.

3. Ren Y, Qiu L, Yuan S, et al. A diagnostic imaging approach for online characterization of multi-impact in aircraft composite structures based on a scanning spatial-wavenumber filter of guided wave. *Mech Syst Signal Process* 2017; 90: 44–63.

4. Hong X, Zhang B, Liu Y, et al. Deep-learning-based guided wave detection for liquid-level state in porcelain bushing type terminal. *Struct Control Health Monit* 2021; 28(1): e2651.

5. Moriot J, Quaegebeur N, Le Duff A, et al. A model-based approach for statistical assessment of detection and localization performance of guided wave-based imaging techniques. *Struct Health Monit* 2018; 17(6): 1460–1472.

6. Zhang B, Hong X and Liu Y. Multi-task deep transfer learning method for guided wave-based integrated health monitoring using piezoelectric transducers. *IEEE Sensors J* 2020; 20(23): 14391–14400.

7. Zhang B, Zhang S and Li W. Bearing performance degradation assessment using long short-term memory recurrent network. *Comput Industry* 2019; 106: 14–29.

8. Zima B and Kędra R. Detection and size estimation of crack in plate based on guided wave propagation. *Mech Syst Signal Process* 2020; 142: 106788.

9. Yelve NP, Mitra M and Mujumdar PM. Detection of delamination in composite laminates using Lamb wave based nonlinear method. *Compos Structures* 2017; 159: 257–266.

10. Leckey CA and Seebo JP. Guided wave energy trapping to detect hidden multilayer delamination damage. *AIP Conf Proc* 2015; 1650: 1162–1169.

11. Eybpoosh M, Berges M and Noh HY. An energy-based sparse representation of ultrasonic guided-waves for online damage detection of pipelines under varying environmental and operational conditions. *Mech Syst Signal Process* 2017; 82: 260–278.

12. Cantero-Chinchilla S, Chiachío J, Chiachío M, et al. A robust Bayesian methodology for damage localization in plate-like structures using ultrasonic guided-waves. *Mech Syst Signal Process* 2019; 122: 192–205.

13. Luo M, Li W, Hei C, et al. Concrete infill monitoring in concrete-filled FRP tubes using a PZT-based ultrasonic time-of-flight method. *Sensors* 2016; 16(12): 2083.

14. Yeung C and Ng CT. Nonlinear guided wave mixing in pipes for detection of material nonlinearity. *J Sound Vibration* 2020; 485: 115541.

15. Cho H, Hasanian M, Shan S, et al. Nonlinear guided wave technique for localized damage detection in plates with surface-bonded sensors to receive Lamb waves generated by shear-horizontal wave mixing. *NDT E Int* 2019; 102: 35–46.

16. Tian Y, Shen Y, Rao D, et al. Metamaterial improved nonlinear ultrasonics for fatigue damage detection. *Smart Mater Structures* 2019; 28(7): 075038.

17. Zhao G, Wang B, Wang T, et al. Detection and monitoring of delamination in composite laminates using ultrasonic guided wave. *Compos Structures* 2019; 225: 111161.

18. Sharif-Khodaei Z and Aliabadi MHF. Lamb-wave based damage detection in anisotropic composite plates. In: *Key Engineering Materials*, Vol. 627. Zürich, Switzerland: Trans Tech Publications Ltd, 2015, pp. 1–4.

19. Sharif Khodaei Z and Aliabadi MH. A multi-level decision fusion strategy for condition based maintenance of composite structures. *Materials* 2016; 9(9): 790.

20. Yang Y, Ng C-T, Kotousov A, et al. Second harmonic generation at fatigue cracks by low-frequency Lamb waves: Experimental and numerical studies. *Mech Syst Signal Process* 2018; 99: 760–773.

21. Mostavi A, Kabir M and Ozevin D. The integration of superlattices and immersion nonlinear ultrasonics to enhance damage detection threshold. *Appl Phys Lett* 2017; 111(20): 201905.

22. Shen Y, Wang J and Xu W. Nonlinear features of guided wave scattering from rivet hole nucleated fatigue cracks considering the rough contact surface condition. *Smart Mater Structures* 2018; 27(10): 105044.

23. Wang J, Shen Y, Rao D, et al. An instantaneous-baseline multi-indicial nonlinear ultrasonic resonance spectral

correlation technique for fatigue crack detection and quantification. *Nonlinear Dyn* 2021; 103(1): 677–698.

24. Hong X, Liu Y, Lin X, et al. Nonlinear ultrasonic detection method for delamination damage of lined anti-corrosion pipes using PZT transducers. *Appl Sci* 2018; 8(11): 2240.

25. Hong X, Liu Y, Liufu Y, et al. Debonding detection in hidden frame supported glass curtain walls using the nonlinear ultrasonic modulation method with piezoceramic transducers. *Sensors* 2018; 18(7): 2094.

26. Hong X, Liu Y, Lin P, et al. Interfacial adhesion-strength detection of structural silicone sealant for hidden frame-supported glass curtain wall based on nonlinear ultrasonic lamb wave. *J Aerospace Eng* 2018; 31(5): 04018047.

27. Lee J, Sheen B and Cho Y. Multi-defect tomographic imaging with a variable shape factor for the RAPID algorithm. *J Visualization* 2016; 19(3): 393–402.

28. Hua J, Lin J and Zeng L. High-resolution damage detection based on local signal difference coefficient model. *Struct Health Monit* 2015; 14(1): 20–34.

29. Dong Wang D, Lin Ye L, Zhongqing Su Z, et al. Probabilistic damage identification based on correlation analysis using guided wave signals in aluminum plates. *Struct Health Monit* 2010; 9(2): 133–144.

30. Wang D, Ye L, Lu Y, et al. Probability of the presence of damage estimated from an active sensor network in a composite panel of multiple stiffeners. *Composites Sci Technology* 2009; 69(13): 2054–2063.

31. Liu X, Bo L, Yang K, et al. Locating and imaging contact delamination based on chaotic detection of nonlinear Lamb waves. *Mech Syst Signal Process* 2018; 109: 58–73.

32. Liu G, Xiao Y, Zhang H, et al. Elliptical ring distribution probability-based damage imaging method for complex aircraft structures. *J Vibroengineering* 2017; 19(7): 4936–4952.

33. Hong M, Su Z, Lu Y, et al. Locating fatigue damage using temporal signal features of nonlinear Lamb waves. *Mech Syst Signal Process* 2015; 60–61: 182–197.

34. Su Z and Hong M. Nonlinear ultrasonics for health monitoring of aerospace structures using active sparse sensor networks. In *Structural health monitoring (SHM) in aerospace structures*, Sawston, Cambridge: Woodhead Publishing, 2016, pp. 353–392.

35. Zeng L, Huang L and Lin J. Damage imaging of composite structures using multipath scattering Lamb waves. *Compos Structures* 2019; 216: 331–339.

36. Moll J, Schulte RT, Hartmann B, et al. Multi-site damage localization in anisotropic plate-like structures using an active guided wave structural health monitoring system. *Smart Materials Structures* 2010; 19(4): 045022.

37. Kundu T, Das S, Martin SA, et al. Locating point of impact in anisotropic fiber reinforced composite plates. *Ultrasonics* 2008; 48(3): 193–201.

38. Liu Y, Hong X and Zhang B. A novel velocity anisotropy probability imaging method using ultrasonic guided waves for composite plates. *Measurement* 2020; 166: 108087.

39. Jones RM *Mechanics of Composite Materials*. Boca Raton, Florida: CRC Press, 2018.

40. Bocchini P, Marzani A and Viola E. Graphical user interface for guided acoustic waves. *J Comput Civil Eng* 2011; 25(3): 202–210.

41. Glushkov E, Glushkova N, Eremin A, et al. Group velocity of cylindrical guided waves in anisotropic laminate composites. *The J Acoust Soc America* 2014; 135(1): 148–154.

42. Chen X, Michaels J and Michaels T. A methodology for estimating guided wave scattering patterns from sparse transducer array measurements. *IEEE Transactions Ultrasonics, Ferroelectrics, Frequency Control* 2015; 62(1): 208–219.

43. Fromme P and Rouge C. Directivity of guided ultrasonic wave scattering at notches and cracks. *J Phys Conf Ser* 2011; 269(1): 012018.